RSC Advances

PAPER

View Article Online
View Journal | View Issue

Cite this: *RSC Adv.*, 2022, **12**, 5042

Facile and green preparation of solid carbon nanoonions *via* catalytic co-pyrolysis of lignin and polyethylene and their adsorption capability towards Cu(II)†

Xiankun Wu,[a] Ting Guo,[a] Ziyan Chen,[a] Zhanghong Wang,*[bc] Kun Qin,[b] Zhikang Wang,[b] Ziqiang Ao,[b] Cheng Yang,*[b] Dekui Shen*[c] and Chunfei Wu*[d]

Carbon nanomaterials, such as carbon nanoonions (CNOs), possess promising applications in various fields. There are urgent demands to synthesize carbon nanomaterials from a green and renewable carbon source. In this study, solid CNOs with relatively uniform size distribution (with diameters of about 30–50 nm), abundant structure defects and oxygen-containing surface functional groups (such as –OH and –COOH) are developed from co-pyrolysis of lignin (LG) and polyethylene (PE) in the presence of Ni-based catalysts. The type of catalyst, the concentration of catalyst and catalytic co-pyrolysis temperature play important roles in the morphologies and properties of CNOs as confirmed by TEM and SEM. Furthermore, the produced CNOs can act as a low-cost and highly-efficient adsorbent to remove Cu(II) from aqueous solution according to a homogeneous monolayer, chemical action-dominated, endothermic and spontaneous process. The theoretical maximum adsorption capacity of CNOs calculated from the Langmuir model is 100.00 mg g^{-1}. Surface deposition, complexation, π electron–cation interaction and electrostatic interaction are responsible for the adsorption of Cu(II) using the prepared CNOs.

Received 8th September 2021
Accepted 16th December 2021

DOI: 10.1039/d1ra06761c

rsc.li/rsc-advances

1 Introduction

Carbon nanomaterials (CNMs) such as carbon nanotubes, graphene, and carbon nanoonions (CNOs) are widely applied in the energy, communication, electronic technology and aerospace industries because of their unique structure and fascinating properties such as favorable thermal and electrical conductivities, low densities and high mechanical strength.[1] During the development of a sustainable social economy and new applications of carbon nanomaterials, there is an increasing market demand for carbon nanomaterials. However, at present the raw materials for commercial preparation of carbon nanomaterials still mainly come from fossil fuels such as coal, oil and their derivatives.[2,3] The limited reserves of fossil fuels and the serious environmental problems caused by the use of fossil fuels urge researchers to look for green and renewable alternatives for the preparation of carbon nanomaterials.

Lignin (LG), one of the most important constituents of biomass, is abundant in carbon (accounting for 50–65% dry LG). Hence, it is a promising candidate for the preparation of carbon-based materials.[4] Although various LG-based carbon materials including biochar, activated carbon, carbon fibers have been successfully produced, the preparation of carbon nanomaterials remains a great challenge due to the complex three-dimensional polymer structure and high oxygen-containing of LG.[5,6] In the process of carbon nanomaterials production, the complex polymer structure of LG is difficult to be destroyed and converted into small molecules. At the same time, the presence of a large amount of oxygen in LG leads to the disordered polycondensation of carbon structure and catalyst poisoning.[7] Recently, it is found that the introduction of hydrogen-rich blends and catalyst in the thermal conversion process of LG can greatly promote the depolymerization of LG, intensify its decomposition and reduce the polycondensation of the intermediate products, resulting in the production of high value-added small molecular chemicals.[8,9] However, there is limited attention paid on the effect of the introduction of hydrogen-rich blends and catalyst on the preparation of carbon materials from LG.[10,11]

[a]*School of Chemistry and Environmental Engineering, Yancheng Teachers University, Yancheng, 224007, PR China*

[b]*College of Eco-Environmental Engineering, Guizhou Minzu University, Guiyang 550025, PR China. E-mail: z.wang2021@hotmail.com; yang-cheng513@163.com*

[c]*Key Laboratory of Energy Thermal Conversion and Control of Ministry of Education, Southeast University, Nanjing 210096, PR China. E-mail: 101011398@seu.edu.cn*

[d]*School of Chemistry and Chemical Engineering, Queen's University Belfast, Belfast BT7 1NN, UK. E-mail: c.wu@qub.ac.uk*

† Electronic supplementary information (ESI) available. See DOI: 10.1039/d1ra06761c

On the other hand, environmental issues arising from heavy metal ions-containing wastewater, such as Cu(II), have attracted more and more attention in recent years due to their horrible toxicity, carcinogenicity and mutagenicity.[12–15] Various technologies, involving chemical precipitation, ion exchange, membrane separation, coagulation and adsorption, have been widely developed to deal with the heavy metal ions-related environment issues. Among these technologies, adsorption is considered as an alternative and promising one in terms of its low cost, high efficiency and ready operation.[16] Carbon nanomaterials, such as CNOs, possess relatively high surface area, developed pore structure, abundant structure defects as well as surface functional groups, are widely accepted as a class of high-efficient adsorbents.[17,18]

Herein, the introduction of PE and nickel (Ni) into the pyrolysis of LG for the preparation of carbon materials and their adsorption capability towards Cu(II) are investigated at present study. Particularly, PE only contains carbon and hydrogen presenting a high effective hydrogen to carbon ratio, which is considered as one of the most typical hydrogen-rich blends.[19] Meanwhile, it has been confirmed that Ni is a low-cost catalyst with good catalytic performance in various fields.[20,21] Our work demonstrate that solid CNOs particles with relatively uniform size (with diameters about 30–50 nm), abundant structure defects and oxygen-containing surface functional groups can be produced from co-pyrolysis of LG and PE with the aid of Ni. Moreover, the as-prepared CNOs possess favorable adsorption capability towards heavy metal ions (Cu(II)) from aqueous solution, which can be attributed to their abundant structure defects and oxygen-containing surface functional groups.

2 Materials and methods

2.1 Materials

LG was extracted from a black liquor collected from an alkali pulping mill in Hunan Province, China according to an acid precipitate method which has been exhaustively described in our previous study.[22] Commercially available PE powder with average M_w of ~4000 and M_n of ~1700 GPC was provided by Sigma-Aldrich Corporation (St. Louis, MO, USA). Chemicals including nickel nitrate hexahydrate (Ni), cobaltous nitrate hexahydrate (Co), iron nitrate nonahydrate (Fe), manganese nitrate tetrahydrate (Mn) and copper nitrate trihydrate in analytical reagent grade were obtained from Sigma-Aldrich Corporation (St. Louis, MO, USA).

2.2 Preparation of carbon materials (CNOs)

The preparation of feedstock and CNOs was in accordance with our previous study.[23,24] In brief, transition metal-loaded LG was firstly prepared by impregnation method, followed by blending PE with the transition metal-loaded LG using an agate mortar. The metal-loaded LG/PE mixture with different types of transition metals and different contents of Ni was readily collected accordingly. For the preparation of CNOs, the feedstock was pyrolyzed at a vertical fixed bed with a heating rate of 10 °C min^{-1} at 800 °C for 2 h. The instrument was allowed to cool down naturally to room temperature after pyrolysis then the carbon products could be collected accordingly. For the investigation on the effect of the type of catalyst, Ni, Co, Fe and Mn in a concentration of 1 mmol g^{-1} were added to treat the mixture of LG and PE; for the effect of the concentration of catalyst, 0–1 mmol g^{-1} of Ni were carried out; for the effect of pyrolysis temperature, 1 mmol Ni/g-treated LG/PE mixture was pyrolyzed at 600, 700, 800 and 900 °C.

2.3 Characterization of CNOs

Morphologic features of the as-synthesized CNOs were characterized using a scanning electron microscopy (SU1510, Hitachi, Japan). Transmission electron microscope (JEM-2010F, JOEL, Japan) equipped with a high-resolution transmission electron microscopy (Talos F200, FEI, USA) was employed to investigate the detailed morphology of CNOs. The crystalline information of CNOs and corresponding catalyst components in CNOs was determined by a powder X-ray diffractometer with Cu Kα radiation in the 2θ range 5–80° (Empyrean Series 2, PANalytical, Netherlands). Surface functional groups of CNOs were analyzed by a Fourier Transform Infrared Spectrometer (Nicolet iS5, Thermo Fisher Scientific, USA). The vibration of the transmissions and corresponding wavenumbers ranging from 600 to 4000 cm^{-1} were collected with a resolution of 4 cm^{-1}. Raman spectroscopy was used to analyze the content of amorphous and graphitized components in CNOs. Particularly, the laser wavelength and wavenumber rang were 523 nm and 500–2500 cm^{-1}. The hysteresis loop of CNOs is determined using a physical property measurement system (PPMS-9, Quantum Design, USA) at room temperature.

2.4 Adsorption of Cu(II) onto CNOs

Stock solution of Cu(II) in a concentration of 1000 mg L^{-1} was prepared by dissolving copper nitrate in deionized water. Cu(II)-Containing solutions in required initial concentrations were subsequently prepared by diluting calculated amount of the stock solution to 50 mL using deionized water in 100 mL conical flasks. About 0.05 mg sample was added the flasks and shook at a horizontal air bath shaker under 25 °C for 8 h with a constant rate of 120 rpm. Afterwards, the suspensions were filtered with 0.22 μm filters and the separated filtrates were analysed by an atomic adsorption spectrometer (FAAS-M6, Thermo, USA) to determine the remnant Cu(II) concentration. The adsorption capacity and removal efficiency were calculated according to ref. 25 and 26. The effect of initial concentrations (ranging from 20 to 200 mg L^{-1}), contact time (ranging from 0–48 h) and ambient temperature (ranging from 15–45 °C) on the adsorption of Cu(II) on samples were investigated. For the investigation of reusability, Cu(II)-loaded CNOs was mixed with 0.1 mol L^{-1} HNO_3 solution and then ultrasonicated at 25 °C for 10 min to desorb. The suspension was filtered. The Cu(II) concentration in filtrate was determined and the filter residue was dried and employed for the renewed adsorption (0.1 g of CNOs was added into 50 mL of Cu(II) solution in a concentration and pH of 80 mg L^{-1} and 5.0, respectively to shake 8 h at 25 °C at

a horizontal air bath shaker). Five repeated adsorption–regeneration cycles were performed.

3 Results and discussion

3.1 Synthesis and characterization of CNOs

As schematically shown in Fig. 1a, carbon materials derived from LG, Ni-loaded LG and LG/PE mixture are amorphous carbons, macro/mesoporous carbons and micro/mesoporous carbons, respectively. Particularly, comparison to LG only, the introduction of Ni into LG can effectively cut off the ether bonds, carbon–carbon bonds and other key bonds to intensify the decomposition of LG and improve the yield of gaseous and liquid products, thus leaving a large amount of pores in relatively large diameters.[27] The pore diameters of Ni-loaded LG based carbons are in the range of 40–120 nm which is assigned to meso and macro pores. For the LG/PE mixture, the introduction of PE can provide a large amount of hydrogen or hydrocarbon radicals, which are effective to the removal of oxygen from LG producing abundant pores with relatively small diameter accordingly (with pore diameters ranging from 2 to 18 nm).[28] Moreover, no carbon product can be collected from the pyrolysis of PE only, which may be related to its low fixed carbon content (<0.5%).[23] In contrast, LG can be readily converted into CNOs with relatively uniform particles after the introduction of PE and Ni (see Fig. 1b). In other words, the co-existence of PE and Ni in LG plays a key role in the preparation of LG-based CNOs. It is reported that the introduction of hydrogen-donor and catalyst makes great influence on the generation of liquid products, improving the yield and selectivity of high value-added fuels or chemicals.[29,30] In this study, the formation of the carbon residue is also remarkably affected by the introduction of hydrogen-donor (PE) and catalyst (Ni) besides to liquid products. For Ni-loaded LG/PE, the deoxygen and decomposition of LG can be enhanced in the presence of the abundant hydrogen or hydrocarbon free radicals provided by PE. Meanwhile, the presence of Ni can further strengthen the synergistic interactions between LG and PE. Afterwards, with the increase of pyrolysis temperature, the interaction between LG and PE gradually ends due to the complete decomposition of PE (about 500 °C), and Ni begins to guide the conversion of amorphous carbon into ordered carbon, resulting in the appearance of CNOs.[24]

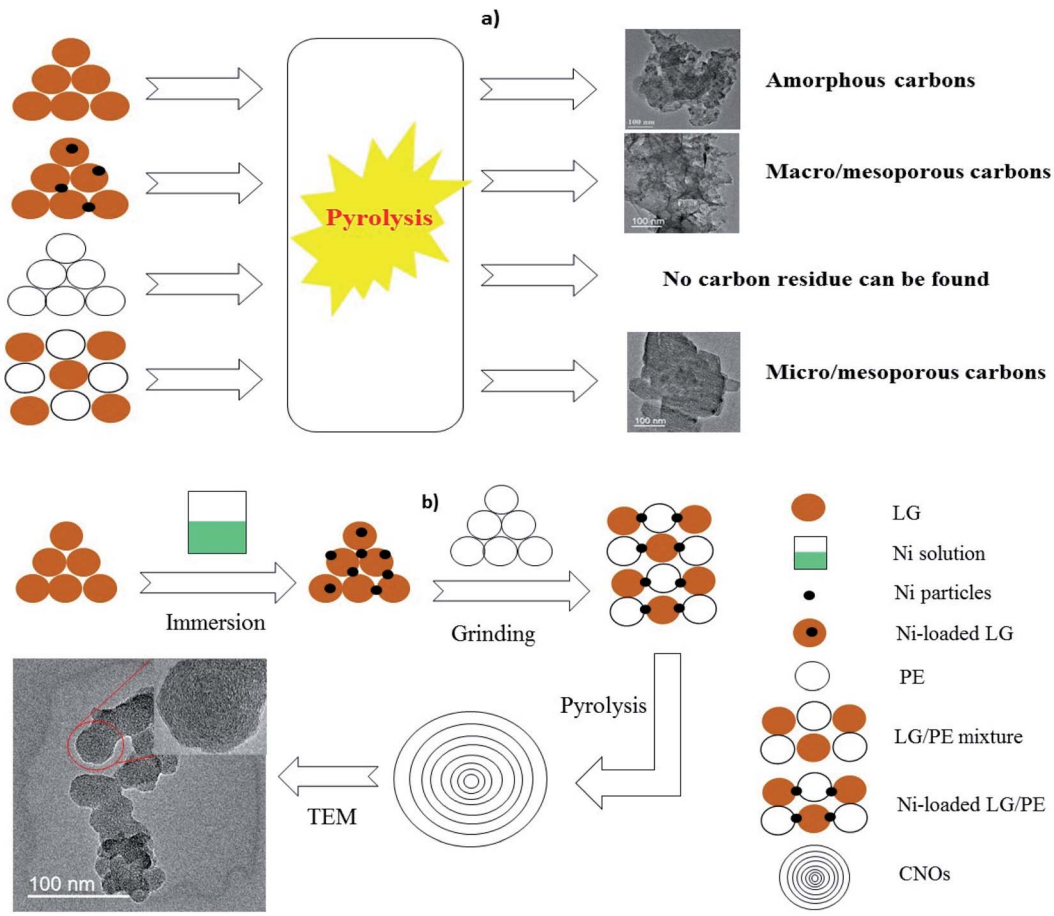

Fig. 1 Schematic illustration of CNOs synthesis. (a) The carbon products of LG, Ni-loaded LG (with a Ni concentration of 1 mmol g^{-1}), PE and LG/PE mixture (with a LG to PE ratio of 1 : 1) prepared with a heating rate of 10 °C min^{-1} at 800 °C for 2 h. (b) The preparation of CNOs *via* co-pyrolysis of LG and PE with the aid of Ni (pyrolysis conditions involving pyrolysis temperature, heating rate and holding time are 800 °C, 10 °C min^{-1} and 2 h, respectively). The Ni concentration in Ni-loaded LG is 2 mmol g^{-1} while the one in Ni-loaded LG/PE is 1 mmol g^{-1} as the mass ratio of LG to PE in the mixture is 1 : 1.

A representative TEM image of as-prepared CNOs is presented in Fig. 2a. The CNOs presents a sphere-like structure and possess a relatively uniform size distribution with diameters in the range of 30–50 nm. HR-TEM (the inset in Fig. 2a) further reveals that the CNOs nanoparticles are made up of concentric graphitic layers with the number of carbon layer of about 20–40. Accordingly, the interlayer spacing of the carbon layers are in the range of 0.33–0.42 nm which is much close to highly ordered planar graphite (0.34 nm).[31] Similarly, the interlayer spacing of the CNOs reported by Adam *et al.* was in the range of 0.27–0.30 nm;[32] the authors proposed that the difference of interlayer spacing between highly ordered planar graphites and the CNOs is greatly related to the degree of ordering as well as the structure curvature. It is worth noting that the line of the interlayer spacing at shell area is evidently clearer than that of the core area in the CNOs (the inset in Fig. 2a). This may reveal the presence of disordered carbon in the CNOs. The unique structure of the CNOs (relatively ordered graphitic carbons as shell and disordered carbon as core) demonstrate that the CNOs can be classified as solid CNOs, which is markedly different from the core–shell structured CNOs (metals acting as core) and hollow CNOs reported in previous studies.[33,34] The imperfect spherical structure (sphere-like structure) and the presence of disordered carbons indicate that the CNOs are abundant in structure defects. The sphere-like structure of the CNOs can be further confirmed by SEM (Fig. 2b). It can be seen that a large amount of CNOs particles are agglomerated together, and some of them fuse with each other to form larger particles.

The XRD patterns of CNOs is shown in Fig. 2c. The peak at a 2θ value of 26.1° can be assigned to the (002) reflection of graphite, which may result from the ordered structure of CNOs.[35] However, the graphite peak in CNOs presents a broad shape, indicating that the crystallinity of the CNOs is relatively limited. The low crystallinity of the CNOs is well in accordance with their abundant structural defects revealed by TEM in Fig. 2a. Moreover, three sharp peaks located at 2θ values of 44.3°, 51.6° and 76.1° can be indexed to the (1 1 1), (2 0 0) and (2 2 0) facets of Ni, respectively. It is reported that the presence of Ni nanoparticles may enable carbon materials with good magnetic property.[36] Accordingly, to investigate the magnetic property of CNOs, a magnetic hysteresis curve is determined at room temperature (Fig. 2d). It can be found that the saturation magnetization of CNOs is 12.4 emu g^{-1} when it is scanned in the magnetic threshold of −10 to 10 kOe, which indicates that the CNOs has a good magnetic property. This is comparable with the Ni-containing onion-like carbon composites obtained from pulsed plasma in a liquid as reported by Abdullaeva *et al.* (with a saturation magnetization of 12.9 emu g^{-1}).[21] The carbon forms (amorphous carbon or graphitic carbon) in CNOs can be further described by Raman spectroscopy (Fig. 2e). The two featured peaks located at 1350 and 1380 cm^{-1} corresponds to the vibration of carbon atoms with dangling bonds in planar terminations of disordered graphite (D) and the vibration of sp^2-bonded carbon atoms in a two-dimensional hexagonal lattice (G), respectively. It is reported that the ratio of the peak intensity between D and G (I_D/I_G) is proportional to the crystalline degree of carbon-based materials.[37] The as calculated I_D/I_G value is 0.89, suggesting that disordered and ordered carbons co-exist in the CNOs. The presence of surface functional groups in CNOs was analyzed using FT-IR spectrum (Fig. 2f). It is found

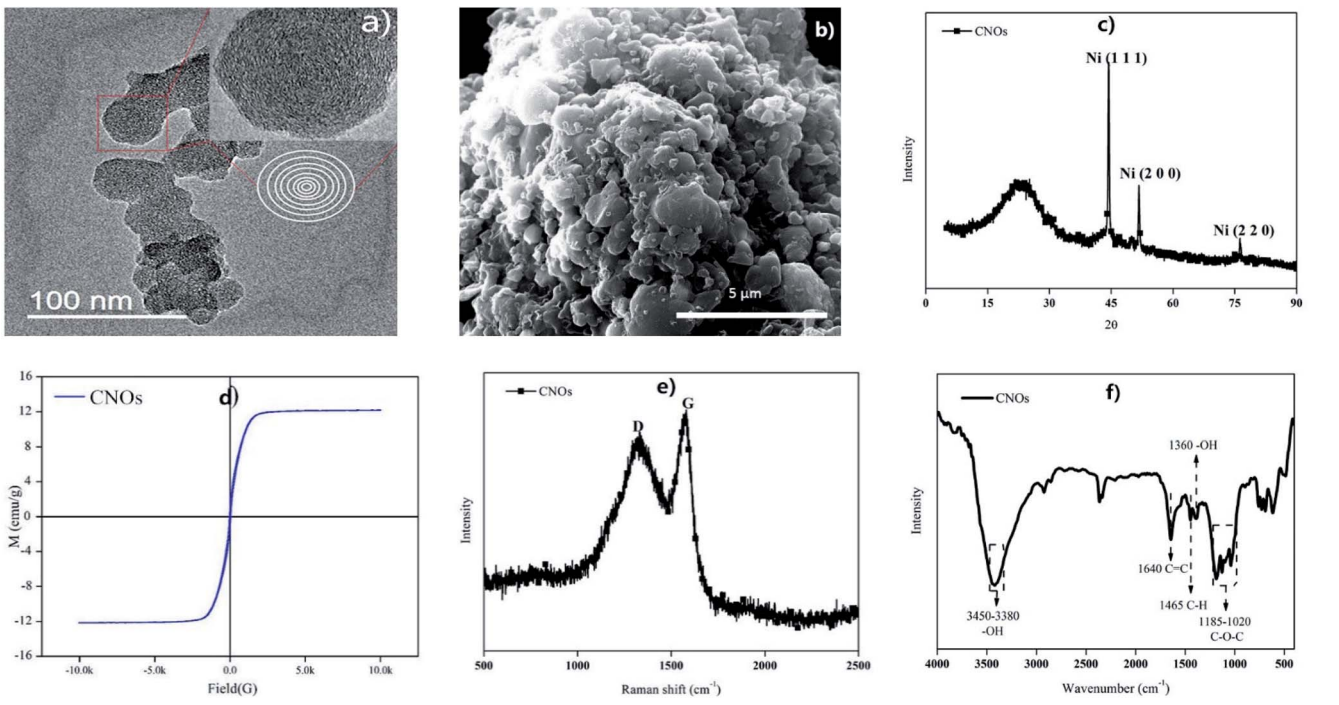

Fig. 2 Characterization of as-prepared CNOs. (a) A typical TEM image of CNOs (the inset is the HR-TEM image showing that the CNOs is composed of about 20–40 carbon layers with a interlayer spacing in the range of 0.33–0.42 nm). (b) SEM image of CNOs. (c) XRD patterns of CNOs. (d) Magnetic hysteresis loop of CNOs. (e) Raman spectrum of CNOs. (f) FT-IR spectrum of CNOs.

that the CNOs contain abundant surface functional groups including oxygen-containing surface functional groups, aromatic C=C and C–H. In detail, the wide and blunt adsorption peak located at 3450–3380 cm^{-1} is attributed to the stretching vibration of hydroxyl (–OH).[38] The vibration of C=C corresponded to the aromatic structure can be observed at 1640 cm^{-1} in CNOs. The adsorption peak at 1465 cm^{-1} is assigned to the C–H stretching vibration in amorphous carbons. The vibration of –OH can be further observed at 1360 cm^{-1} as well. The wide peak in the wavenumber range of 1120–1020 cm^{-1} is mainly caused by the stretching vibration of carboxyl (–COOH).

3.2 Effect of preparing conditions on the synthesis of CNOs

It is reported that preparing conditions such the type of catalyst, the concentration of catalyst and pyrolysis temperature play important roles in the morphology and property of carbon products.[39,40] Herein, the effects of the type of catalyst, the concentration of catalyst and pyrolysis temperature on the preparation of CNOs are investigated. Fig. 3 shows the TEM and SEM images of the carbon materials prepared using different transition metals including Co (Fig. 3a and b), Fe (Fig. 3c and d) and Mn (Fig. 3e and f). As shown in Fig. 3a and b, the carbon materials prepared from Co-loaded LG/PE is found to be folded sheet-like graphene clusters with a thickness of 1–4 nm. For Fe-loaded LG/PE (Fig. 3c and d), the carbon products present a fiber-like and hollow structure, which hence can be considered as carbon nanotubes. The inner diameters, outer diameters and length of the carbon nanotubes are 60–80 nm, 70–90 nm and 1–3 μm, respectively. Moreover, the metal particles with a diameter of about 60–100 nm are found at the tip of the carbon nanotubes, which suggests that the carbon nanotubes may mainly grow *via* the mechanism of tip-growth.[41] The carbon product derived from Mn-loaded LG/PE presents as the clusters of smooth paper-like sheets with a thickness of 0.5–1 nm, which can be assigned to graphene-like carbons (Fig. 3e and f).

According to Fig. 2, the introduction of Ni with a concentration of 1 mmol g^{-1} into LG/PE can result in the production of CNOs. The effect of Ni concentration ranging of 0.25 to 0.75 mmol g^{-1} is further investigated as follows (Fig. 4). It is found that the as-prepared carbon materials mainly presents a bulk irregular shape as the Ni concentration employed is 0.25 mmol g^{-1} (Fig. 4a and b). No fine nanostructure (CNOs) can be found, which may be attributed to without enough catalyst to destroy the carbon matrix and guide the growth of CNOs at present Ni concentration. This is similar to the effect of catalyst concentration on the preparation of other carbon nanomaterials.[42] With the increase of the Ni concentration in LG/PE to 0.5–0.75 mmol g^{-1}, CNOs can be readily found in the carbon products (Fig. 4c–f). The diameters of the 0.5 mmol g^{-1} Ni-loaded LG/PE and 0.75 mmol g^{-1} Ni-loaded LG/PE derived CNOs are in the range of 60–120 nm and 40–100 nm, respectively. Accordingly, it can be summarized that the increase of catalyst concentration is favorable for producing finely structured CNOs.

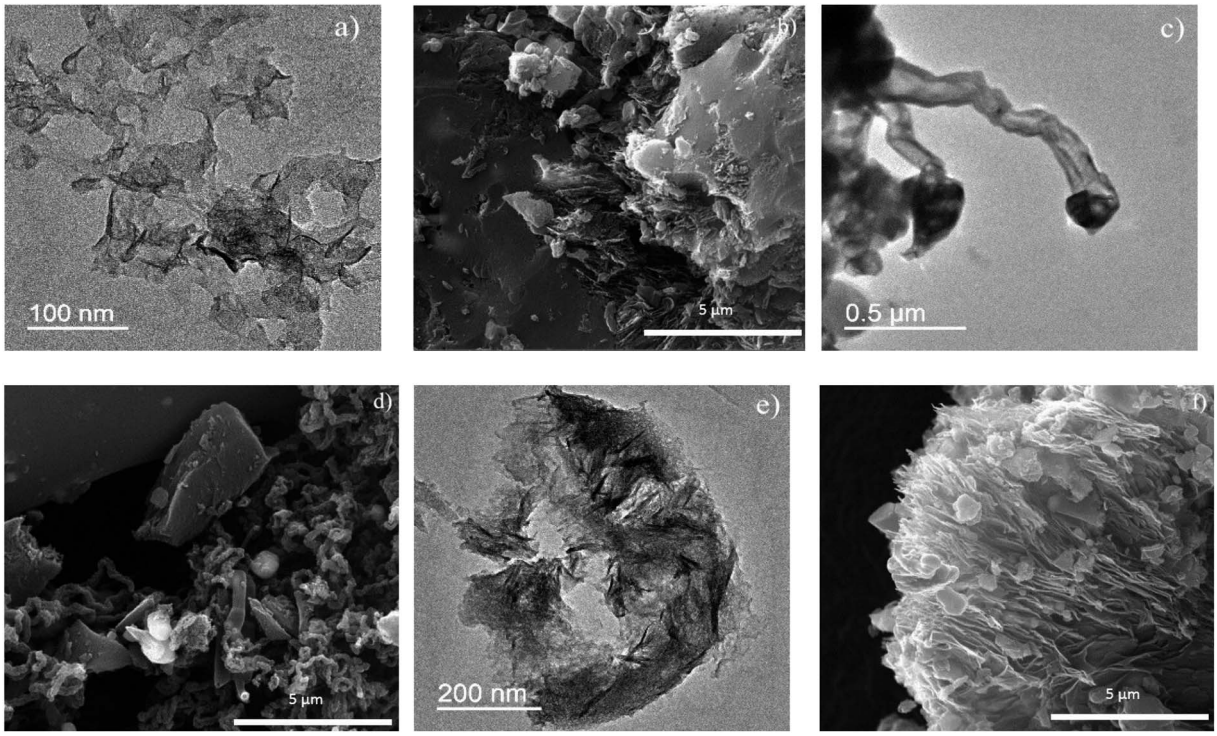

Fig. 3 Effect of transition metal types on the preparation of carbon nanomaterials from catalytic co-pyrolysis of LG/PE. (a) and (b) are the TEM and SEM images of the carbon nanomaterial prepared from Co (Co-loaded LG/PE), respectively. (c) and (d) are the TEM and SEM images of the carbon nanomaterial prepared from F (Fe-loaded LG/PE), respectively. (e) and (f) are the TEM and SEM images of the carbon nanomaterial prepared from Mn (Mn-loaded LG/PE), respectively.

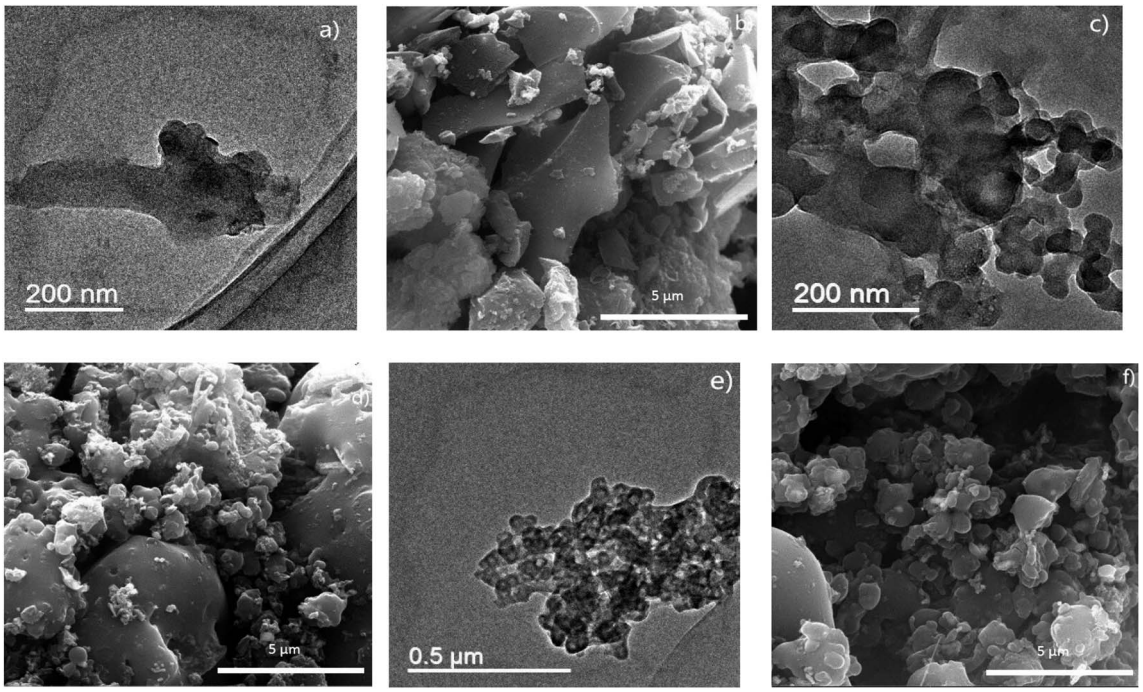

Fig. 4 Effect of Ni loading on the preparation of carbon nanomaterials from catalytic co-pyrolysis of LG/PE. (a) and (b) are the TEM and SEM images of the carbon nanomaterial prepared from a Ni loading of 0.25 mmol g^{-1}, respectively. (c) and (d) are the TEM and SEM images of the carbon nanomaterial prepared from a Ni loading of 0.5 mmol g^{-1}, respectively. (e) and (f) are the TEM and SEM images of the carbon nanomaterial prepared from a Ni loading of 0.75 mmol g^{-1}, respectively.

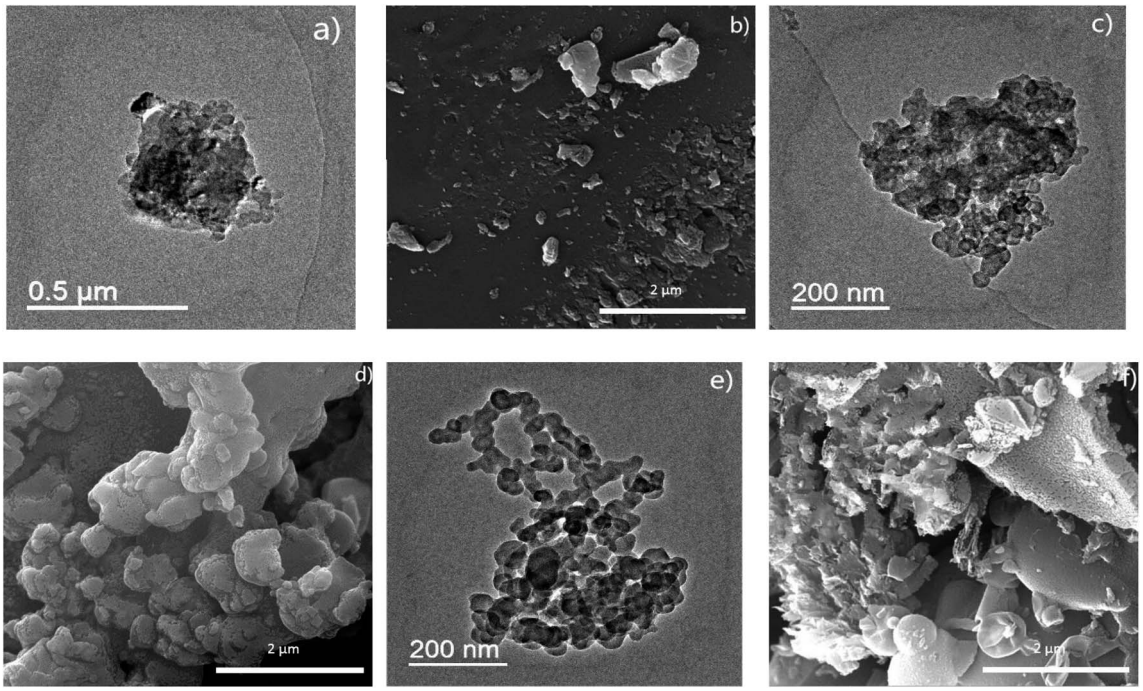

Fig. 5 Effect of pyrolysis temperature on the preparation of carbon nanomaterials from catalytic co-pyrolysis of LG/PE. (a) and (b) are the TEM and SEM images of the carbon nanomaterial prepared from 600 °C, respectively. (c) and (d) are the TEM and SEM images of the carbon nanomaterial prepared from 700 °C, respectively. (e) and (f) are the TEM and SEM images of the carbon nanomaterial prepared from 900 °C, respectively.

The TEM and SEM images of the carbon products prepared under 600, 700 and 900 °C is showed in Fig. 5. As shown, no fine nanostructure can be found in the carbon derived at 600 °C (Fig. 5a and b). This may be ascribed to the relatively low activity of the catalyst at present temperature. With the increase of pyrolysis temperature (700 °C), a small amount of CNOs particles with the diameters in the range of 30–50 nm can be found (Fig. 5c and d). It is worth mentioning that most of the carbon materials derived at 700 °C still remains an irregular shape, suggesting that 700 °C is not the appropriate temperature for CNOs preparation. The CNOs prepared under 900 °C present the diameters in the range of 25–55 nm (Fig. 5e and f). This may indicate that the increase of pyrolysis temperature is beneficial for the preparation of CNOs.

3.3 Adsorption performance of CNOs

The adsorption capability of CNOs towards Cu(II) from aqueous solution is employed to evaluate its adsorption performance.

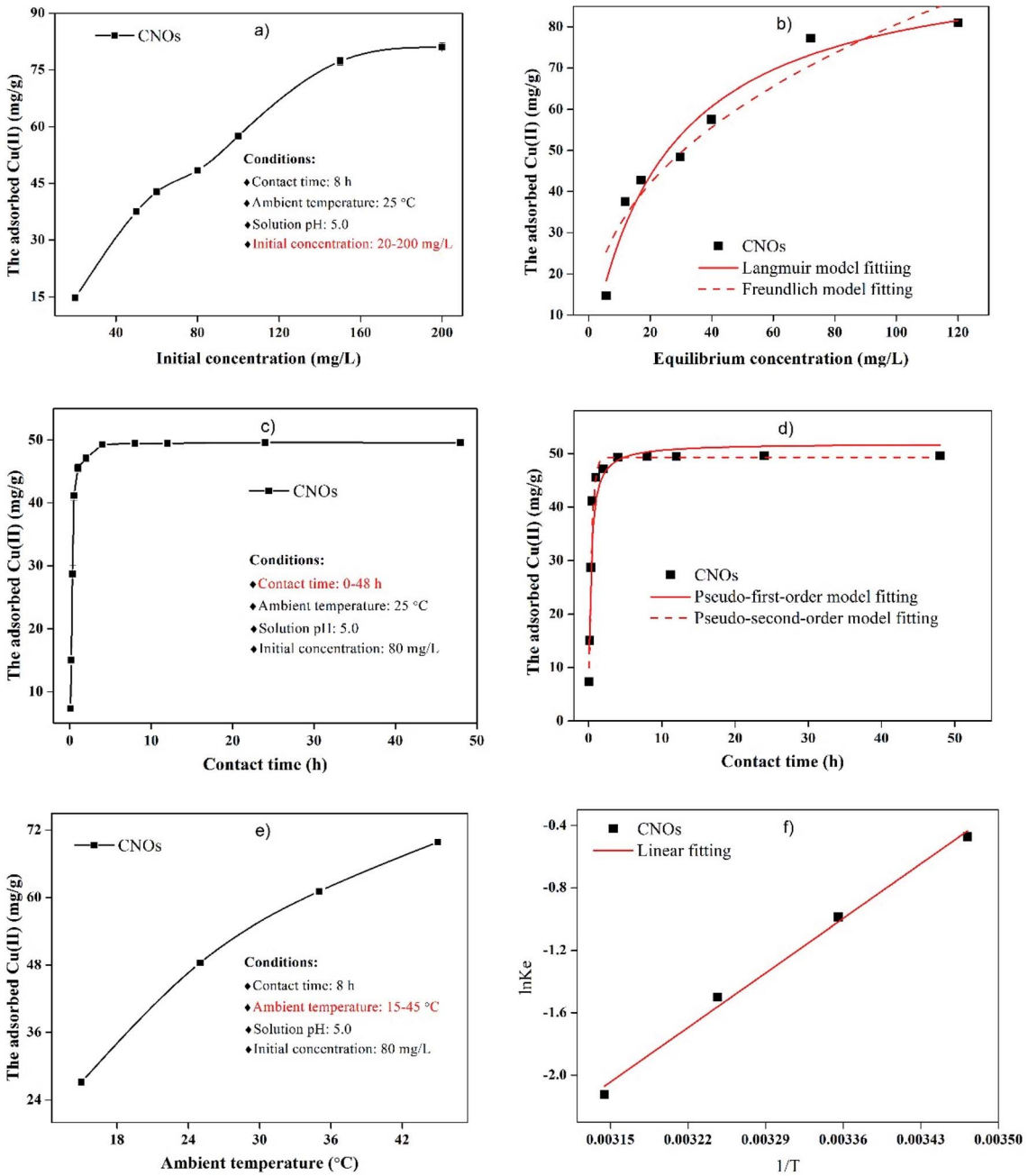

Fig. 6 Adsorption performance of CNOs towards Cu(II) from aqueous solution. (a) Effect of initial concentration of Cu(II) on the adsorption of Cu(II) using CNOs (20–200 mg L^{-1}). (b) Adsorption process fitted by Langmuir model and Freundlich model. (c) Effect of contact time on the adsorption of Cu(II) using CNOs (0–48 h). (d) Adsorption process fitted by pseudo-first-order model and pseudo-second-order model. (e) Effect of ambient temperature on the adsorption of Cu(II) using CNOs (15–45 °C). (f) Thermodynamic analysis (the relationship between $1/T$ and ln K_e).

Table 1 Adsorption isotherm, kinetic and thermodynamic parameters of Cu(II) adsorption by CNOs (corresponding equations are presented in ESI)

Adsorption isotherm					
Langmuir model			Freundlich model		
Q_m (mg g^{-1})	K_l (L mg^{-1})	R^2	K_f (mg$^{(1-n)}$ L^n g^{-1})	n	R^2
100.00	26.80	0.983	12.52	2.47	0.918
Adsorption kinetic					
Pseudo-first-order model			Pseudo-second-order model		
q_{exp} (mg g^{-1})	k_1 (h^{-1})	q_e (mg g^{-1}) R^2	k_2 (g (mg h)$^{-1}$)	q_e (mg g^{-1})	R^2
49.74	2.70	48.92 0.980	0.11	49.75	0.999
Thermodynamic analysis					
ΔG^0 (kJ mol^{-1})				ΔH^0 (kJ mol^{-1})	ΔS^0 (J (mol K)$^{-1}$)
288 (K)	298 (K)	308 (K)	318 (K)		
−8.50	−11.51	−13.80	−16.25	65.09	256.13

Fig. 6a shows that the adsorbed Cu(II) onto CNOs is increased with the initial Cu(II) concentration. The adsorption capacity of Cu(II) onto CNOs is 14.74 mg g^{-1} when the Cu(II) initial concentration is 20 mg L^{-1}. While the adsorption capacity of 80.96 mg g^{-1} can be obtained from the Cu(II) initial concentration of 200 mg L^{-1}. Adsorption isotherm fitting presented in Fig. 6b and Table 1 reveals that the adsorption can be well described by Langmuir model with a good correlation coefficient (R^2) of 0.983 in comparison with that of Freundlich model (0.918), indicating that the adsorption of Cu(II) onto CNOs is assigned to a homogeneous monolayer adsorption.[43] The theoretical maximum adsorption capacity of CNOs calculated from Langmuir model is 100.00 mg g^{-1} which is comparable with those of g-C_3N_4/graphene oxide hydrogel and alginate hydrogels, and is obviously higher than those of sawdust-chitosan nanocomposite beads and chitosan/Al_2O_3/Fe_3O_4 nanocomposite (see Table 2).[16,44–46] The adsorption effected by contact time is shown in Fig. 6c. It can be found that Cu(II) is rapidly adsorbed by CNOs at the initial 1 h, in which more than 90% of Cu(II) is removed. Then, the adsorption gradually slows down and reaches a equilibrium at about 4 h. Kinetic analysis (Fig. 6d) reveals that compared to pseudo-first-order model, the pseudo-second-order model can give a good simulation on the adsorption process (with a R^2 value closed to 1), confirming that the Cu(II) adsorption process is mainly dominated by a chemisorption process (see Table 1).[47] Fig. 6e shows that the adsorption of Cu(II) using CNOs is positively related to the ambient temperature, suggesting that the adsorption process possesses an endothermic nature.[48] Moreover, Gibbs free energy (ΔG^0) calculated from thermodynamic equations (see ESI†) presents negative values at each ambient temperature (−8.50 to −16.25 kJ mol^{-1}), which reveals that the adsorption is a spontaneous reaction (see Table 1).[49]

Due to the good magnetic property of CNOs has been confirmed in Fig. 2f, we herein attempt to separate the CNOs after Cu(II) adsorption using a external magnetic field (the insert in Fig. 7). It is found that the post-adsorption CNOs can be readily separated from the suspension with a permanent magnet. This is of great significance to the collection and

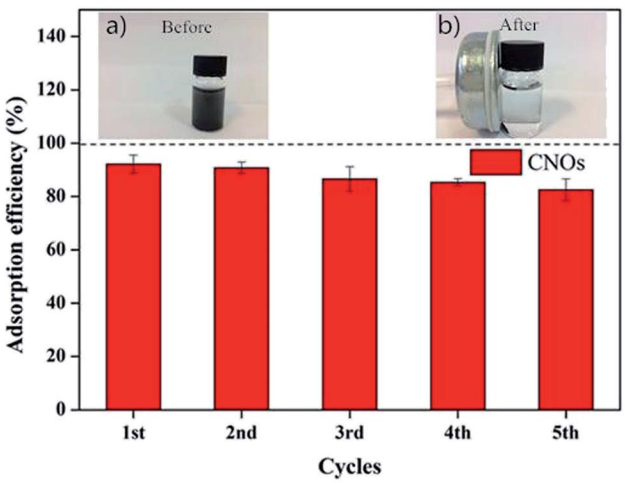

Fig. 7 Recycling utilization of CNOs for Cu(II) adsorption in 5 cycles. The inset (a) is the suspension of the adsorption of Cu(II) onto CNOs and (b) is the magnetic separation of the CNOs after Cu(II) adsorption.

Table 2 Comparison of the maximum capacity of Cu(II) adsorption

Adsorbents	Maximum adsorption capacity (mg g^{-1})	Conditions	Ref.
g-C_3N_4/graphene oxide hydrogel	128–160	pH 5.0, 25 °C, 24 h	44
Rich husk@mesoporous silica MCM-41	91.4	pH 5.5, 25 °C, 2 h	50
Sawdust-chitosan nanocomposite beads	7.32	pH 5.0, 30 °C, 70 min	16
Chitosan/Al_2O_3/Fe_3O_4 nanocomposite	30.97	pH 5.5, 25 °C, 24 h	45
f-Sporopollenin microcapsules	22.71	pH 6, 25 °C, 2 h	51
PE/PP non-woven fabric grafted with poly(bis[2-(methacryloyloxy)ethyl] phosphate)	35.96	pH 5, 25 °C, 4 h	52
Alginate hydrogels	111.79	pH 5, 25 °C, 24 h	46
Alginate-based composite beads	64.14	pH 5, 25 °C, 8 h	53
CNOs	100.00	pH 5, 25 °C, 24 h	Present study

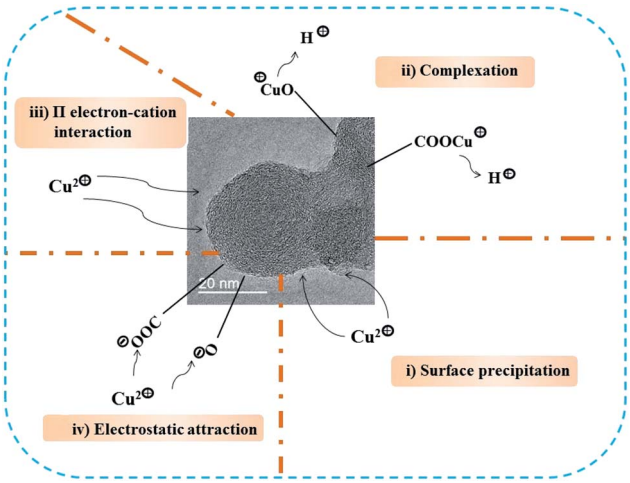

Fig. 8 The proposed mechanism for Cu(II) adsorption onto CNOs.

further recycling of the adsorption sediment. Based on the good magnetic separation property, the cycling utilization of the CNOs for Cu(II) adsorption is investigated. The result of five successive adsorption–regeneration cycles of Cu(II) loaded CNOs is showed in Fig. 7. As shown, more than 80% adsorption efficiency is maintained after five cycles, indicating that the CNOs is rather resusable.

It is well established that the physico-chemical properties of an adsorbent plays important roles in its adsorption capability.[47] The CNOs shows a favorable adsorption capability towards Cu(II), which may be highly related to their structure and surface properties. Moreover, the adsorption kinetic and thermodynamic analysis reveals that the adsorption of Cu(II) onto CNOs belongs to a chemical action-dominated, endothermic and spontaneous process. Accordingly, based on the properties of CNOs, it is inferred that the following adsorption interactions may be involved in the adsorption of Cu(II) (see Fig. 8). (i) Surface deposition. The abundant structure defects of CNOs greatly increases its surface roughness which can be in favor of the adsorption of Cu(II) *via* surface deposition.[54] (ii) Complexation. The abundant oxygen-containing surface functional groups of CNOs such as –OH and –COOH can provide a large amount of effectively active sites to immobilize Cu(II) through the release of H^+ with equivalent charge.[55] (iii) π electron–cation interaction. The aromatic structure, especially for aromatic C=C, can act as π-donor to combine with Cu(II) based on the strong affinity of them.[56] In addition, electrostatic interaction may make certain contribution to the adsorption of Cu(II) as well.

4 Conclusion

Solid CNOs can be readily prepared from co-pyrolysis of lignin (LG) and polyethylene (PE) in the presence of Ni-based catalysts. The size distribution of the CNOs is in the range of 30–50 nm and 20–40 carbon layers are involved. XRD and Raman spectrum reveal that the CNOs possess abundant structure defects. The CNOs contain a large amount of surface functional groups, such as –OH, –COOH, C=C and C–H as confirmed by FT-IR analysis. The CNOs with a saturation magnetization of 12.4 emu g^{-1} reveals that the CNOs presents a good magnetic property. Folded sheet-like graphene clusters, carbon nanotubes and smooth paper-like sheets can be collected as Co, Fe and Mn are employed as catalysts, respectively. The increase of catalyst concentration (0.25–1 mmol g^{-1}) and catalytic co-pyrolysis temperature (600–900 °C) are favorable for the preparation of CNOs. The adsorption of Cu(II) onto the CNOs can be well fitted by Langmuir model and the theoretical maximum adsorption capacity is 100.00 mg g^{-1}. Pseudo-second-order model gives a good simulation to the adsorption process and reveals a chemical action-dominated nature. Thermodynamic analysis shows that the adsorption of Cu(II) onto the CNOs is ascribed to an endothermic and spontaneous process. Surface deposition, complexation, π electron–cation interaction and electrostatic interaction are involved during the adsorption of Cu(II) using the CNOs.

Author contributions

Xiankun Wu: methodology, analysis, writing. Ting Guo: analysis. Ziyan Chen: investigation. Zhanghong Wang: methodology, investigation, supervision, writing – original draft. Kun Qin: methodology, writing – original draft. Zhikang Wang: methodology, writing – original draft. Ziqiang Ao: methodology, investigation. Cheng Yang: writing – review & editing. Dekui Shen: supervision, investigation, writing – review & editing. Chunfei Wu: supervision, investigation, writing – review & editing.

Conflicts of interest

The authors declare that they have no known competing financial interests or personal relationships that could have appeared to influence the work reported in this paper.

Acknowledgements

The authors greatly acknowledge the funding support from the projects supported by National Natural Science Foundation of China (Grant no. 51676047 and 41867048), Guizhou Provincial Science-Technology Support Plan Projects ([2018]2807 and [2020]4Y017), the Science and Technology Foundation of Guizhou Province [2019]1155, Jiangsu College Students' Innovation and Entrepreneurship Training Program (202010324075Y), the scientific research fund of Guizhou Minzu University (GZMUZK [2021]YB13), the scientific research platform of Guizhou Minzu University (GZMUGCZX[2021]02) and the construction projected of Key Laboratory of State Ethnic Affairs Commission ([2020] No. 91 of DDA office, *i.e.* The Karst Environmental Geological Hazard Prevention Laboratory of Guizhou Minzu University).

References

1 Z. Wang, D. Shen, C. Wu and S. Gu, *Green Chem.*, 2018, **20**, 5031–5057.

2 X. Cui, W. Wei and W. Chen, *Carbon*, 2010, **48**, 2782–2791.
3 Y. Chen and J. Yu, *Carbon*, 2005, **43**, 3183–3186.
4 Y. Ge, Z. Li, Y. Kong, Q. Song and K. Wang, *J. Ind. Eng. Chem.*, 2014, **20**, 4429–4436.
5 S. Gillet, M. Aguedo, L. Petitjean, A. R. C. Morais, A. M. da Costa Lopes, R. M. Lukasik and P. T. Anastas, *Green Chem.*, 2017, **19**, 4200–4233.
6 S. Chatterjee and T. Saito, *ChemSusChem*, 2015, **8**, 3941–3958.
7 J.-M. Ha, K.-R. Hwang, Y.-M. Kim, J. Jae, K. H. Kim, H. W. Lee, J.-Y. Kim and Y.-K. Park, *Renewable Sustainable Energy Rev.*, 2019, **111**, 422–441.
8 H. Zhang, R. Xiao, J. Nie, B. Jin, S. Shao and G. Xiao, *Bioresour. Technol.*, 2015, **192**, 68–74.
9 O. Sanahuja-Parejo, A. Veses, M. V. Navarro, J. M. López, R. Murillo, M. S. Callén and T. García, *Energy Convers. Manage.*, 2018, **171**, 1202–1212.
10 Y. Xu, G. Q. Luo, S. W. He, F. F. Deng, Q. C. Pang, Y. Q. Xu and H. Yao, *Fuel*, 2019, **239**, 982–990.
11 Y. Xu, X. Zeng, G. Luo, B. Zhang, P. Xu, M. Xu and H. Yao, *Fuel*, 2016, **183**, 73–79.
12 M. Shaban, M. R. Abukhadra and A. Hamd, *Clean Technol. Environ. Policy*, 2017, **20**, 13–28.
13 M. Shaban, M. R. Abukhadra, A. Hamd, R. R. Amin and A. Abdel Khalek, *J. Environ. Manage.*, 2017, **204**, 189–199.
14 H. S. Mohamed, N. K. Soliman, A. F. Moustafa, O. F. Abdel-Gawad, R. R. Taha and S. A. Ahmed, *Int. J. Environ. Anal. Chem.*, 2021, **101**, 1850–1877.
15 M. Shaban, A. Hamd, R. R. Amin, M. R. Abukhadra, A. A. Khalek, A. A. P. Khan and A. M. Asiri, *Environ. Sci. Pollut. Res. Int.*, 2020, **27**, 32670–32682.
16 K. Kayalvizhi, N. M. I. Alhaji, D. Saravanakkumar, S. B. Mohamed, K. Kaviyarasu, A. Ayeshamariam, A. M. Al-Mohaimeed, M. R. AbdelGawwad and M. S. Elshikh, *Environ. Res.*, 2022, **203**, 111814.
17 V. Dhand, J. S. Prasad, M. V. Rao, S. Bharadwaj, Y. Anjaneyulu and P. K. Jain, *Mater. Sci. Eng., C*, 2013, **33**, 758–762.
18 E. Tovar-Martinez, J. A. Moreno-Torres, J. V. Cabrera-Salazar, M. Reyes-Reyes, L. F. Chazaro-Ruiz and R. López-Sandoval, *Carbon*, 2018, **140**, 171–181.
19 S. D. Anuar Sharuddin, F. Abnisa, W. M. A. Wan Daud and M. K. Aroua, *Energy Convers. Manage.*, 2016, **115**, 308–326.
20 A. I. Almendros, G. Blázquez, A. Ronda, M. A. Martín-Lara and M. Calero, *Renewable Energy*, 2017, **103**, 825–835.
21 Z. Abdullaeva, E. Omurzak, C. Iwamoto, H. S. Ganapathy, S. Sulaimankulova, C. Liliang and T. Mashimo, *Carbon*, 2012, **50**, 1776–1785.
22 D. Shen, J. Zhao, R. Xiao and S. Gu, *J. Anal. Appl. Pyrolysis*, 2015, **111**, 47–54.
23 Z. Wang, D. Shen, C. Wu and S. Gu, *Energy Convers. Manage.*, 2018, **172**, 32–38.
24 Z. Wang, G. Liu, D. Shen, C. Wu and S. Gu, *J. Energy Inst.*, 2020, **93**, 281–291.
25 A. Hamd, A. R. Dryaz, M. Shaban, H. AlMohamadi, K. A. Abu Al-Ola, N. K. Soliman and S. A. Ahmed, *Nanomaterials*, 2021, **11**, 2441.
26 N. K. Soliman, A. F. Moustafa, H. R. A. El-Mageed, O. F. Abdel-Gawad, E. T. Elkady, S. A. Ahmed and H. S. Mohamed, *Sci. Rep.*, 2021, **11**, 10000.
27 R. H. Venderbosch, *ChemSusChem*, 2015, **8**, 1306–1316.
28 X. Zhang, H. Lei, S. Chen and J. Wu, *Green Chem.*, 2016, **18**, 4145–4169.
29 B. Zhang, Z. Zhong, K. Ding and Z. Song, *Fuel*, 2015, **139**, 622–628.
30 Y. Xue, A. Kelkar and X. Bai, *Fuel*, 2016, **166**, 227–236.
31 M. Sevilla, G. A. Ferrero and A. B. Fuertes, *Energy Storage Materials*, 2016, **5**, 33–42.
32 M. Adam, A. Hart, L. A. Stevens, J. Wood, J. P. Robinson and S. P. Rigby, *Carbon*, 2018, **138**, 427–435.
33 Y. Zheng and P. Zhu, *RSC Adv.*, 2016, **6**, 92285–92298.
34 C. He, N. Zhao, C. Shi, X. Du and J. Li, *Mater. Chem. Phys.*, 2006, **97**, 109–115.
35 L. Sun, C. Tian, M. Li, X. Meng, L. Wang, R. Wang, J. Yin and H. Fu, *J. Mater. Chem. A*, 2013, **1**, 6462.
36 A. Manukyan, A. Elsukova, A. Mirzakhanyan, H. Gyulasaryan, A. Kocharian, S. Sulyanov, M. Spasova, F. Römer, M. Farle and E. Sharoyan, *J. Magn. Magn. Mater.*, 2018, **467**, 150–159.
37 M. Sevilla, C. Sanchís, T. Valdés-Solís, E. Morallón and A. B. Fuertes, *J. Phys. Chem. C*, 2007, **111**, 9749–9756.
38 L. Zhao, X. Cao, O. Mašek and A. Zimmerman, *J. Hazard. Mater.*, 2013, **256–257**, 1–9.
39 W.-J. Liu, K. Tian, Y.-R. He, H. Jiang and H.-Q. Yu, *Environ. Sci. Technol.*, 2014, **48**, 13951–13959.
40 E. Thompson, A. E. Danks, L. Bourgeois and Z. Schnepp, *Green Chem.*, 2015, **17**, 551–556.
41 J.-P. Tessonnier and D. S. Su, *ChemSusChem*, 2011, **4**, 824–847.
42 V. B. Mohan, K. T. Lau, D. Hui and D. Bhattacharyya, *Composites, Part B*, 2018, **142**, 200–220.
43 Z. Wang, H. Guo, F. Shen, G. Yang, Y. Zhang, Y. Zeng, L. Wang, H. Xiao and S. Deng, *Chemosphere*, 2015, **119**, 646–653.
44 Y. Feng, G. Chen, Y. Zhang, D. Li, C. Ling, Q. Wang and G. Liu, *J. Hazard. Mater.*, 2022, **424**, 127362.
45 F. Karimi, A. Ayati, B. Tanhaei, A. L. Sanati, S. Afshar, A. Kardan, Z. Dabirifar and C. Karaman, *Environ. Res.*, 2022, **203**, 111753.
46 Z. Li, Z. Guo, T. Zhang, Q. Li, J. Chen, W. Ji, C. Liu and Y. Wei, *Colloids Surf., B*, 2021, **207**, 112036.
47 Z. Wang, D. Shen, F. Shen and T. Li, *Chemosphere*, 2016, **150**, 1–7.
48 Z. Wang, D. Shen, F. Shen, C. Wu and S. Gu, *Int. Biodeterior. Biodegrad.*, 2017, **120**, 104–114.
49 M. Kılıç, Ç. Kırbıyık, Ö. Çepelioğullar and A. E. Pütün, *Appl. Surf. Sci.*, 2013, **283**, 856–862.
50 Y. Gao, R.-y. Zhou, L. Yao, W. Yin, J.-x. Yu, Q. Yue, Z. Xue, H. He and B. Gao, *J. Hazard. Mater.*, 2022, **424**, 127203.
51 A. Bilgic, *Colloids Surf., A*, 2021, **631**, 127658.
52 Y. Limsuwan, T. Rattanawongwiboon, P. Lertsarawut, K. Hemvichian and T. Pongprayoon, *J. Environ. Chem. Eng.*, 2021, **9**, 106440.

53 D. Zhao, W. Ye and W. Cui, *Environ. Sci. Pollut. Res.*, 2021, DOI: 10.1007/s11356-021-17013-4.
54 D. S. Su, X. Chen, G. Weinberg, A. Klein-Hofmann, O. Timpe, S. B. A. Hamid and R. Schlögl, *Angew. Chem., Int. Ed.*, 2005, **44**, 5488–5492.
55 Z. Wang, F. Shen, D. Shen, Y. Jiang and R. Xiao, *J. Environ. Sci.*, 2017, **53**, 293–300.
56 Z. Wang, D. Shen, F. Shen, C. Wu and S. Gu, *J. Mol. Liq.*, 2017, **241**, 612–621.